Deep Impact: Observations from a Worldwide Earth-Based Campaign

K. J. Meech,[1]* N. Ageorges,[2] M. F. A'Hearn,[3] C. Arpigny,[4] A. Ates,[5] J. Aycock,[6] S. Bagnulo,[2] J. Bailey,[7] R. Barber,[8] L. Barrera,[9] R. Barrena,[10] J. M. Bauer,[11] M. J. S. Belton,[12] F. Bensch,[13] B. Bhattacharya,[14] N. Biver,[15] G. Blake,[14] D. Bockelée-Morvan,[15] H. Boehnhardt,[16] B. P. Bonev,[17] T. Bonev,[18] M. W. Buie,[19] M. G. Burton,[20] H. M. Butner,[21] R. Cabanac,[22] R. Campbell,[6] H. Campins,[23] M. T. Capria,[24] T. Carroll,[21] F. Chaffee,[6] S. B. Charnley,[25] R. Cleis,[26] A. Coates,[27] A. Cochran,[28] P. Colom,[15] A. Conrad,[6] I. M. Coulson,[21] J. Crovisier,[15] J. deBuizer,[29] R. Dekany,[14] J. de Léon,[10] N. Dello Russo,[30] A. Delsanti,[1] M. DiSanti,[31] J. Drummond,[26] L. Dundon,[1] P. B. Etzel,[32] T. L. Farnham,[3] P. Feldman,[33] Y. R. Fernández,[23] M. D. Filipovic,[34] S. Fisher,[35] A. Fitzsimmons,[36] D. Fong,[37] R. Fugate,[26] H. Fujiwara,[38] T. Fujiyoshi,[39] R. Furusho,[40] T. Fuse,[39] E. Gibb,[41] O. Groussin,[3] S. Gulkis,[11] M. Gurwell,[37] E. Hadamcik,[42] O. Hainaut,[2] D. Harker,[43] D. Harrington,[1] M. Harwit,[44] S. Hasegawa,[45] C. W. Hergenrother,[46] P. Hirst,[21] K. Hodapp,[1] M. Honda,[45] E. S. Howell,[47] D. Hutsemékers,[4] D. Iono,[37] W.-H. Ip,[48] W. Jackson,[49] E. Jehin,[2] Z. J. Jiang,[50] G. H. Jones,[16] P. A. Jones,[51] T. Kadono,[52] U. W. Kamath,[53] H. U. Käufl,[2] T. Kasuga,[54] H. Kawakita,[55] M. S. Kelley,[56] F. Kerber,[2] M. Kidger,[10] D. Kinoshita,[48] M. Knight,[3] L. Lara,[57] S. M. Larson,[46] S. Lederer,[58] C.-F. Lee,[37] A. C. Levasseur-Regourd,[42] J. Y. Li,[3] Q.-S. Li,[50] J. Licandro,[10,59] Z.-Y. Lin,[48] C. M. Lisse,[30] G. LoCurto,[2] A. J. Lovell,[60] S. C. Lowry,[36] J. Lyke,[6] D. Lynch,[61] J. Ma,[50] K. Magee-Sauer,[62] G. Maheswar,[53] J. Manfroid,[4] O. Marco,[2] P. Martin,[22] G. Melnick,[37] S. Miller,[8] T. Miyata,[38] G. H. Moriarty-Schieven,[21] N. Moskovitz,[1] B. E. A. Mueller,[63] M. J. Mumma,[31] S. Muneer,[53] D. A. Neufeld,[33] T. Ootsubo,[64] D. Osip,[65] S. K. Pandea,[53] E. Pantin,[66] R. Paterno-Mahler,[5] B. Patten,[37] B. E. Penprase,[5] A. Peck,[37] G. Petitas,[37] N. Pinilla-Alonso,[67] J. Pittichova,[1] E. Pompei,[2] T. P. Prabhu,[53] C. Qi,[37] R. Rao,[37] H. Rauer,[68] H. Reitsema,[69] S. D. Rodgers,[25] P. Rodriguez,[70] R. Ruane,[26] G. Ruch,[56] W. Rujopakarn,[71] D. K. Sahu,[53] S. Sako,[38] I. Sakon,[38] N. Samarasinha,[63] J. M. Sarkissian,[51] I. Saviane,[2] M. Schirmer,[59] P. Schultz,[72] R. Schulz,[73] P. Seitzer,[71] T. Sekiguchi,[54] F. Selman,[2] M. Serra-Ricart,[10] R. Sharp,[74] R. L. Snell,[75] C. Snodgrass,[36] T. Stallard,[8] G. Stecklein,[5] C. Sterken,[76] J. A. Stüwe,[77] S. Sugita,[38] M. Sumner,[14] N. Suntzeff,[63] R. Swaters,[3] S. Takakuwa,[37] N. Takato,[39] J. Thomas-Osip,[65] E. Thompson,[26] A. T. Tokunaga,[1] G. P. Tozzi,[78] H. Tran,[6] M. Troy,[11] C. Trujillo,[29] J. Van Cleve,[69] R. Vasundhara,[53] R. Vazquez,[79] F. Vilas,[80] G. Villanueva,[16] K. von Braun,[81] P. Vora,[82] R. J. Wainscoat,[1] K. Walsh,[3] J. Watanabe,[54] H. A. Weaver,[33] W. Weaver,[26] M. Weiler,[68] P. R. Weissman,[11] W. F. Welsh,[32] D. Wilner,[37] S. Wolk,[37] M. Womack,[83] D. Wooden,[25] L. M. Woodney,[58] C. Woodward,[56] Z.-Y. Wu,[50] J.-H. Wu,[50] T. Yamashita,[39] B. Yang,[1] Y.-B. Yang,[50] S. Yokogawa,[37] A. C. Zook,[5] A. Zauderer,[3] X. Zhao,[50] X. Zhou,[50] J.-M. Zucconi[84]

On 4 July 2005, many observatories around the world and in space observed the collision of Deep Impact with comet 9P/Tempel 1 or its aftermath. This was an unprecedented coordinated observational campaign. These data show that (i) there was new material after impact that was compositionally different from that seen before impact; (ii) the ratio of dust mass to gas mass in the ejecta was much larger than before impact; (iii) the new activity did not last more than a few days, and by 9 July the comet's behavior was indistinguishable from its pre-impact behavior; and (iv) there were interesting transient phenomena that may be correlated with cratering physics.

The Deep Impact mission was designed so that much of the mission-critical science would be done from Earth-based telescopes. These facilities would observe the comet before, during, and after impact to follow the evolution of the comet in wavelength regimes and time scales inaccessible to the spacecraft. Observations began in 1997 to characterize the nucleus of comet 9P/Tempel 1 for mission planning and to establish a baseline of normal behavior against which impact-induced changes could be assessed (1, 2). From 1997 through 2004, observations on 229 nights were obtained from 14 telescopes at nine observatories. In 2005, since the comet came out of solar conjunction, the worldwide collaboration has involved more than 550 whole or partial nights of observation using 73 Earth-based telescopes at 35 observatories (Fig. 1), plus many (Earth-orbital and Sun-orbital) space-based facilities.

Here we give an overview of the scientific conclusions and collective observations from the Earth-based campaign (3). As seen from Earth, the Deep Impact event did not create a new period of sustained cometary activity, and in many ways the artificial impact looked very much like a natural outburst. There were some observable changes after impact in the chemistry of the observed dust and gas as well as in the physical properties of the dust, which may suggest that the material beneath the surface was different in composition from the surface materials.

Ejecta cloud. The ejecta cloud was first resolved ~20 min after impact by Earth-orbiting telescopes at visible and ultraviolet wavelengths. Later, ground-based telescopes worldwide imaged the southwesterly-expanding cloud of dust and gas in the visible and infrared (IR) wavelength regime ($\lambda = 0.3$ to 13 μm). Generally, the visible and near-IR wavelengths (0.3 to 2.5 μm) achieved the best spatial resolution and sensitivity; that is, most observations were sampling the reflected sunlight from dust in the cloud, with some contribution from the gas in emission bands (<0.6 μm).

About 1 hour after impact, the ejecta was semicircular and extended across position angles 145° to 325°. The ejecta cloud had a nonuniform light distribution. During the first 20 hours after impact, the time series of images showed the leading edge of the dust cloud expanding outward at a projected speed of ~200 ± 20 m/s (although varying with azimuth). The southward orientation of the ejecta indicates that the impact occurred below the orbital plane of the comet.

From 6 July 2005 (all dates are UT) onward, the expanding dust cloud increasingly changed shape because of the push of solar radiation pressure, forcing the particles into the tail (i.e., antisolar) direction at a position angle of 110°.
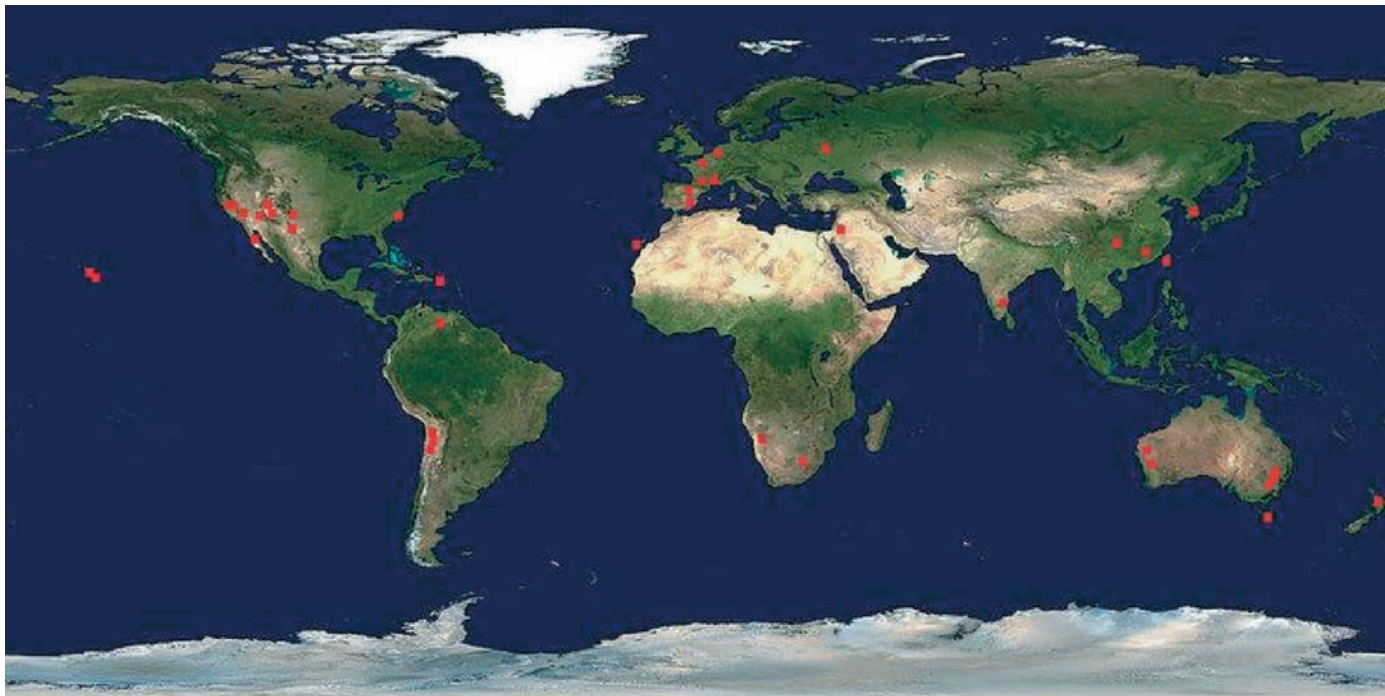
Fig. 1. Map of Earth, showing the locations of observatories collaborating in the coordinated campaign (red dots). World map credit: NASA.

The maximum projected distance in the sunward direction was 30,000 km, achieved on 7 July (Fig. 2). Together, the projected speed and projected distance imply that a typical dust grain experienced a ratio of radiation pressure to gravity of ~0.3.

The size-sorting of the dust grains by radiation pressure led to color changes in the ejecta cloud. Bluer colors on the tailward side of the plume suggested that submicrometer dust grains—which are more sensitive to radiation pressure and less efficient in reflecting red and IR light—were pushed out first. By 9 July, the dust cloud dispersed and had faded below the detection limit of many imaging instruments (Fig. 2).

By assuming a dust albedo and a "typical" grain size (0.5 μm), the flux of the impact ejecta can be converted into a total dust mass. On the order of ~10^6 kg of dust were liberated, equivalent to ~10 hours of normal (preimpact) dust production.

Coma structures. For the 6 months before impact, the dust coma showed a broad fan to the southeast and other narrow jetlike radial features at various azimuths. Because they did not vary with the rotation of the nucleus, these

[1]Institute for Astronomy, University of Hawaii at Manoa, 2680 Woodlawn Drive, Honolulu, HI 96822, USA. [2]European Southern Observatory, Casilla 19001, Santiago 19, Chile. [3]University of Maryland, College Park, MD 20742, USA. [4]Université de Liège, B-4000 Liège, Belgium. [5]Pomona College, Claremont, CA 91711, USA. [6]Keck Observatory, Kamuela, HI 96743, USA. [7]Australian Centre for Astrobiology, Macquarie University, Sydney, NSW 2109, Australia. [8]University College London, London WC1E 6BT, UK. [9]Universidad Metropolitana de Ciencias de la Educación, Ñuñoa, Santiago, Chile. [10]Instituto de Astrofísica de Canarias, E38200 La Laguna (Tenerife), Spain. [11]NASA/Jet Propulsion Laboratory, Pasadena, CA 91109, USA. [12]Belton Space Initiatives, Tucson, AZ 85716, USA. [13]Radioastronomisches Institut der Universität Bonn, D-53121 Bonn, Germany. [14]California Institute of Technology, Pasadena, CA 91125, USA. [15]Observatoire Paris Meudon, F-92195 Meudon, France. [16]Max-Planck-Institut für Sonnensystemforschung, Katlenburg-Lindau 37191, Germany. [17]University of Toledo, Toledo, OH 43606, USA. [18]Institute of Astronomy, Sofia 1784, Bulgaria. [19]Lowell Observatory, Flagstaff, AZ 86001, USA. [20]University of New South Wales, Sydney, NSW 2052, Australia. [21]Joint Astronomy Centre, Hilo, HI 96720, USA. [22]Canada-France-Hawaii Telescope, Kamuela, HI 96743, USA. [23]University of Central Florida, Orlando, FL 32816, USA. [24]Instituto di Astrofisica Spaziale e Fisica Cosmica, 00133 Roma, Italy. [25]NASA Ames Research Center, Moffett Field, CA 94035, USA. [26]Air Force Research Lab, Kirtland Air Force Base, NM 87117, USA. [27]Mullard Space Science Laboratory, Surrey RH5 6NT, UK. [28]University of Texas, Austin, TX 78712, USA. [29]Gemini Observatory, Casilla 603, La

Serena, Chile. [30]Johns Hopkins University Applied Physics Laboratory, Laurel, MD 20723, USA. [31]NASA/Goddard Space Flight Center, Greenbelt, MD 20770, USA. [32]San Diego State University, San Diego, CA 92182, USA. [33]Johns Hopkins University, Baltimore, MD 21218, USA. [34]University of Western Sydney, NSW 1797, Australia. [35]Gemini Observatory North, Hilo, HI 96720, USA. [36]Queen's University, Belfast BT7 1NN, UK. [37]Harvard-Smithsonian Center for Astrophysics, Cambridge, MA 02138, USA. [38]University of Tokyo, Tokyo 113-8654, Japan. [39]Subaru Telescope, Hilo, HI 96720, USA. [40]Waseda University, Tokyo 169-8050, Japan. [41]University of Notre Dame, South Bend, IN 46556, USA. [42]Service d'Aéronomie, CNRS, 91371 Verrières Le Buisson, France. [43]University of California, San Diego, La Jolla, CA 92093, USA. [44]Cornell University, Ithaca, NY 14853, USA. [45]Institute of Space and Astronautical Science, Sagamihara, Kanagawa 229-8510, Japan. [46]University of Arizona, Tucson, AZ 85721, USA. [47]Arecibo Observatory, Arecibo, PR 00612, USA. [48]National Central University, Jhongli, Taoyuan 32001, Taiwan. [49]University of California, Davis, CA 95616, USA. [50]National Astronomical Observatories, Beijing 100012, China. [51]Australia Telescope National Facility, Epping, NSW 1710, Australia. [52]Japan Agency for Marine-Earth Science and Technology, Yokosuka, Kanagawa 237-0061, Japan. [53]Indian Institute of Astrophysics, Bangalore 560 034, India. [54]National Astronomical Observatory of Japan, Tokyo 181-8588, Japan. [55]Kyoto Sangyo University, Kyoto 603-8555, Japan. [56]University of Minnesota, Minneapolis, MN 55455, USA. [57]Instituto de Astrofísica de Andalucía–CSIC, 18080 Granada, Spain. [58]California State University, San Bernardino, CA 92407, USA. [59]Isaac

Newton Group of Telescopes, La Palma E-38700, Spain. [60]Agnes Scott College, Atlanta, GA 30030, USA. [61]Aerospace Corporation, Los Angeles, CA 90009, USA. [62]Rowan University, Glassboro, NJ 08028, USA. [63]National Optical Astronomy Observatory, Tucson, AZ 85719, USA. [64]Nagoya University, Nagoya 464-8601, Japan. [65]Las Campanas Observatory, Pasadena, CA 91101, USA. [66]CEA-Service d'Astronomie, Saclay F-91191, France. [67]Fundación Galileo Galilei & Telescopio Nazionale Galileo, La Palma 38700, Spain. [68]Deutsches Zentrum für Luft- und Raumfahrt, Berlin 12489, Germany. [69]Ball Aerospace, Boulder, CO 80306, USA. [70]European Space Agency, Villafranco del Castillo, 28080 Madrid, Spain. [71]University of Michigan, Ann Arbor, MI 48109, USA. [72]Brown University, Providence, RI 02912, USA. [73]European Space Agency, Noordwijk NL-2200 AG, Netherlands. [74]Anglo-Australian Observatory, Epping, NSW 1710, Australia. [75]University of Massachusetts, Amherst, MA 01003, USA. [76]University of Brussels, B-1050 Brussels, Belgium. [77]Leiden Observatory, NL-2300 RA Leiden, Netherlands. [78]Osservatorio Astrofisico di Arcetri, Firenze I-50125, Italy. [79]Universidad Nacional Autónoma de México, Ensenada 22800, Mexico. [80]NASA/Johnson Space Center, Houston, TX 77058, USA. [81]Carnegie Institution of Washington, Washington, DC 20015, USA. [82]College of William and Mary, Williamsburg, VA 23187, USA. [83]St. Cloud State University, St. Cloud, MN 56301, USA. [84]Observatoire de Besançon, 25010 Besançon Cedex, France.

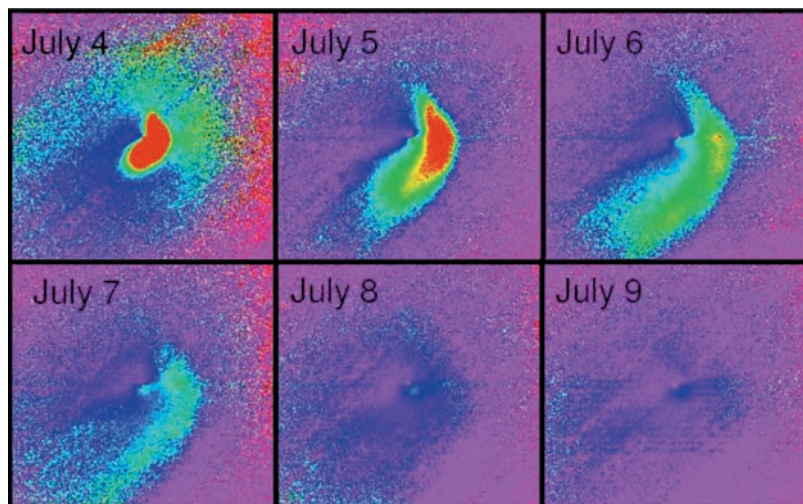*To whom correspondence should be addressed. E-mail: meech@ifa.hawaii.edu

Fig. 2. Sequence of processed post-impact *R* band images of the dust coma of 9P/Tempel 1 acquired from the Nordic Optical Telescope. North is up and east is left. Dates are UT; the first image was taken ~16 hours after impact, and succeeding images were taken around the same time of day on the following nights. The width of each panel is ~120,000 km at the comet. Each image has been divided by a pre-impact 3 July image to accentuate structure in the coma. The evolution of the ejecta cloud is clearly seen.

features are interpreted as a fan coma emanating from localized sources on the nucleus, with the observer point of view being outside the emission cone (*4*, *5*). Neither the number of jets and fans nor their orientations changed during the impact period. In particular, no new long-lived jet or fan has been identified as being from the newly excavated crater.

Fluctuations that were observed in the intensity of some coma structures are possibly related to the impact event itself but could also be due to natural variations in activity. A southwesterly jetlike feature seen one-half rotation period after impact was observed to be brighter than it had been before impact. This could have been caused by gas production from the ejecta dust grains themselves. By just one full rotation period after impact (41 hours), the coma morphology had returned to its pre-impact state, which suggests that the impact site was by this time beginning to cease its activity.

Gas production. The gas species commonly monitored at visible wavelengths in cometary comae—CN, C_2, C_3, NH_2, and CH—were observed in 9P/Tempel 1 before and after impact. During the first 2 days after impact, observations showed the intensity of the species' emission bands increasing by a factor of ~1.5 to 5. An example of the increase in CN as seen through spectroscopy is shown in Fig. 3. Photometry was also used by some groups (*6*). The abundance ratios among the common species stayed at pre-impact levels (*5*). In particular, the C_2-to-CN abundance ratio of ~0.8 classifies 9P/Tempel 1 as a "typical" comet (*7*), as it was before impact. Gas production was back to its pre-impact level by 9 July.

In the near-IR, species not directly detectable before impact—H_2O, C_2H_6, CH_3OH, C_2H_2, and HCN—appeared after impact (*8*).

The abundance ratios among these species were consistent with those of typical Oort cloud comets (*8*), although 9P/Tempel 1 is a Jupiter-family comet. There have been relatively few studies of these species among members of the Jupiter family.

Measurements of the CN (0-0) band in the visible spectra revealed isotopic abundances of carbon and nitrogen: The $^{12}C/^{13}C$ ratio was close to the solar value (which is 89), and the $^{14}N/^{15}N$ ratio was half that of Earth's value (which is 272). Hence, comet 9P/Tempel 1 shows the same low nitrogen isotopic ratio that was recently detected in other Jupiter-family comets (*9*).

In addition to near-IR detections of water, other groups monitored the submillimeter transitions of H_2O and the near-ultraviolet transitions of OH. For example, spacecraft observing the 557-GHz transition of water reported a 20% increase in the hours after impact. However, the natural variations in water production that were seen before impact could account for this. On the other hand, there was also a factor of 3 increase in OH production. The reconciliation of these data awaits further analysis.

Several species were monitored from ground-based radio telescopes. HCN at 88.6 and 265.9 GHz and CH_3OH at 145 GHz were detected for only a few days after impact; the production rates later returned to or fell below pre-impact levels. The abundance ratios of HCN and CH_3OH relative to water were similar to those observed in other comets. Post-impact upper limits to production rates were derived for CO, CS, H_2CO, and H_2S; pre-impact upper limits were obtained for OH, CH_3OH, and HCN. All radio detections and upper limits with space-based and ground-based telescopes indicated very little effect on molecular gas produc-

tion as a result of the impact, whereas somewhat larger effects were noticeable in H-, C-, and N-bearing molecules and in the dust detectable in the visible and near-IR wavelength region. A possible explanation for this different behavior could be gas released from the ejected cometary dust as a consequence of dust fragmentation due to the sublimation of intergrain ices.

Wide-angle imaging in narrowband filters tuned to the fluorescence of H_2O^+ and CO^+ in visible wavelengths was performed. The observations did not reveal any signatures of substantial ion production that could be attributed to the impact.

X-ray observations (0.1 to 1.0 keV) were performed at impact time and afterward. Comets produce x-rays by charge-exchange reactions between the solar wind's highly ionized minor ion population and the neutral cometary gas species (*10*). A ~30% increase in the x-ray counts, lasting for about 1 day, was seen by Earth-orbiting x-ray telescopes after impact. This is interpreted as due to excursions in the comet's gas production rate for a collisionally thin charge-exchange system.

Dust properties. Mid-IR observations can be used to constrain fundamental properties of cometary dust, and 9P/Tempel 1 was no exception, at least after impact. Because of the comet's faintness, pre-impact mid-IR spectra (λ = 8 to 13 μm) obtained from the ground were essentially flat and featureless. Space-based observations gave better signal but yielded a similar pre-impact picture. The grains were generally large (>1 μm) and the 8- to 13-μm emission band was very weak, consistent with previous apparitions (*11*).

Immediately after impact, a short barlike structure extending ~1 arc sec at a position angle of ~225° was seen from ground-based mid-IR imaging. Over the next several hours, the mid-IR flux of the central coma brightened by a factor of ~2 (Fig. 4). Note that the increase in total dust flux (compared to the apparently more modest increase in gas flux) implies that the ratio of dust mass to gas mass in the ejecta was not the same as that seen before impact. This was a dusty impact.

Ground-based mid-IR spectroscopy revealed a substantial growth in the 8- to 13-μm silicate emission feature after impact. The strength of that emission band suggests an emission dominated by submicrometer (0.5 to 1 μm) dust grains. The small size of the grains is consistent with the reports from the spacecraft imaging (*12*). The composition, as derived from modeling the shape of the emission band, is a mix of amorphous olivine and pyroxene, amorphous carbon (which controls the dust temperature), crystalline forsterite, and clino- and orthopyroxene (*13*, *14*). In particular, the resonance peak seen at 11.2 μm is indicative of Mg-rich crystalline olivine. Indeed, the degree of crystallinity in the dust grains was substantially higher in the impact ejecta relative to pre-impact measurements. Organic refractory

material was not needed to model the emission band. The shape of the post-impact silicate feature is strikingly similar to the spectra of active, long-period comets, especially Hale-Bopp. The silicate emission band persisted for about 20 to 26 hours after impact; after that time, the spectral features had disappeared and the comet had returned to its pre-impact mid-IR flux.

Space-based mid-IR observations were performed in phase with the rotation period to ensure that the comet was sampled at similar states of activity. Moreover, in the wavelength segments that are inaccessible from the ground (5 to 8 µm, 13 to 18 µm, and >25 µm), the space-based data filled in the gaps. Imaging at $\lambda = 16$ µm at the time of impact may have revealed thermal emission from the hot impact plume, albeit with a spatial resolution that was poorer than that of the ground-based telescopes by a factor of 5 to 10. Spectroscopic coverage of the entire 5- to 40-µm region after impact revealed compositional and grain temperature information similar to what was seen on the ground. The 9- to 37-µm region showed evidence of crystalline pyroxene in addition to the olivine seen from the ground. Spectral features due to H_2O, CO_2, and carbonaceous material were also seen (*15*).

Polarization of the dust coma was monitored by several groups. Before impact, polarization in visible wavelengths was measured to be $7.0 \pm 0.5\%$. After impact, some variation of polarization with wavelength (0.65 to 0.9 µm) and also with distance from the nucleus was seen, suggesting a change in grain size, porosity, or composition.

Photometric behavior. The transient photometric behavior of the comet's inner coma in the first 15 to 30 min after impact was recorded by many groups. For a small aperture of radius ~1 arc sec, the comet brightened by about 2.3 mag in the visible wavelengths. Note that the nucleus had a magnitude of ~17 in standard Cousins R band at the time of impact.

Subtle changes in the light curve can be linked to post-impact phenomena on the comet's surface. A typical light curve with high temporal resolution is shown in Fig. 5. In the first few minutes, there were three distinct rates of brightening. From impact to ~1 min after, the comet brightened sharply. Then, for the next 6 min, the brightening rate was more gradual. However, at ~7 min after impact, the brightening rate increased again, although not as steeply as at first. This rate remained constant for the next 10 to 15 min, at which point the comet's flux began to level off. In the smallest apertures (radius ≈ 1 arc sec), the flux then began to decrease again ~45 min after impact.

This three-sloped light curve as seen in Fig. 5 could be directly linked to the formation of the impact crater, its evolution, and the evolution of the outgassing from it. The falloff in brightness by the first few hours after impact is related to a decrease in the level of activity from the new crater. However, the effect is also partly due to

the ejecta moving beyond the edge of the photometric aperture; the peak of the light curve depends strongly on aperture size. Light curves from larger apertures displayed later times of peak brightness; moreover, the comet did not stay at its peak brightness for very long, regardless of aperture. This means that the outgassing from the crater, although much less fecund relative to its activity immediately after impact, had not completely ceased. If it had, light curves with large apertures would show a flat peak flux lasting for the length of time needed for the dust to move out of the aperture.

No group reported seeing an unambiguous, short-duration (<1 s) flash at the exact moment of impact, despite the impact site being visible from Earth. This is likely due to the low contrast of the flash versus the rest of the light from the inner coma as seen in most Earth-based telescopes.

Natural outbursts. The comet was observed to have a series of natural outbursts in addition to the one induced by Deep Impact.

These outbursts were identifiable above the comet's normal, gradual brightening as it approached perihelion. The brightness of the comet's dust coma varied with heliocentric distance r as $r^{-6.7}$ until early May and dropped thereafter. The first identified outburst occurred on 23 and 24 February (*16*) as the comet brightened by ~40%.

Morphological analysis of an outburst was carried out from visible-wavelength images obtained on 14 June. The outburst showed an arc of material extending over position angles of 215° to 45°. At the peak of the outburst, the comet's brightness was higher than that in previous dates by ~50 to 60%. This outburst was also seen by the Deep Impact spacecraft itself. Observations by multiple telescopes allowed a projected velocity of the dust from the outburst to be calculated: ~200 m/s. Note that this is similar to the speed of the Deep Impact ejecta.

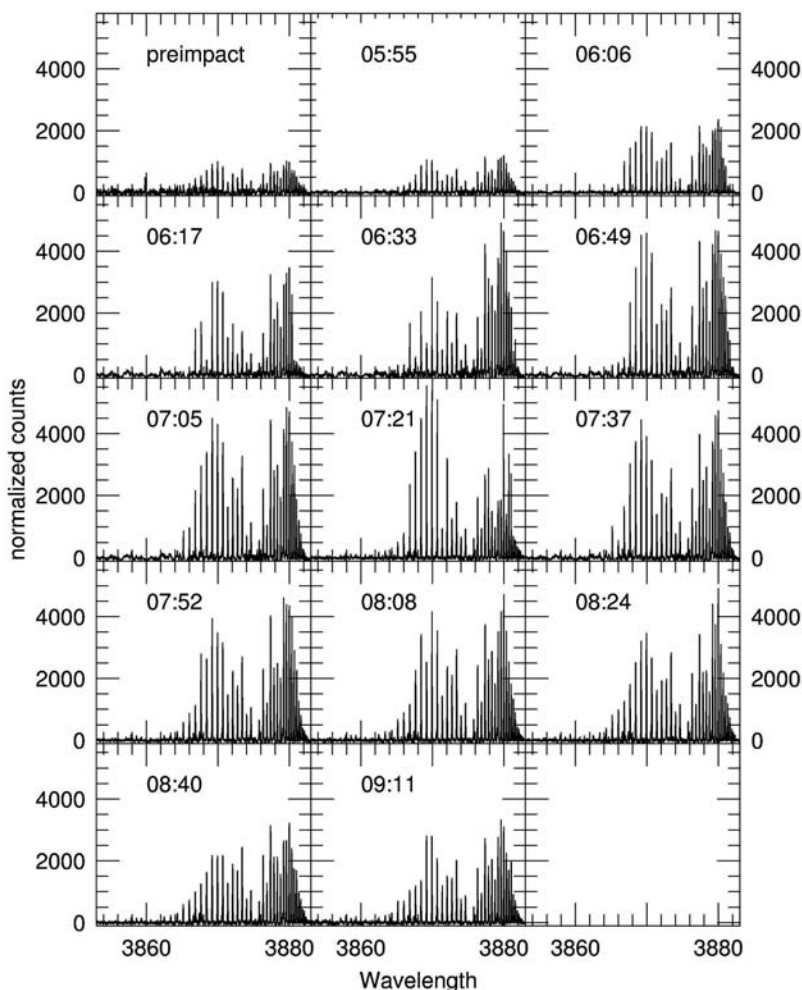After this discovery, more intense photometric monitoring was initiated, and a series

Fig. 3. Spectra (normalized to 1 air mass and 15 min exposure time) of the CN $\Delta v = 0$ emission band ($\delta v = 0$) on 4 July 2005. Data were obtained with the Keck I telescope. The plot shows that the intensity of the CN lines increased by more than a factor of 5 from the pre-impact level to the peak post-impact level (UT 07:21, ~1.5 hours after impact). The emission then begins to decrease; the ejecta must have filled the slit, and the decrease represents the dilution of the gas by expansion. This is consistent with a gas outflow velocity of ~1.1 km/s.

of outbursts occurred approximately every 8 days. On 22 June, there was another outburst and the dust coma morphology was similar to the one on 14 June. On 29 June, mid-IR and x-ray observations revealed another outburst.

On 2 July, another outburst was reported by the spacecraft and by several observers. This was the only event for which a submillimeter continuum detection was obtained; no such detection was reported for the impact event itself. An outburst that was seen by ground-based radio observations of OH occurred on 6 July. Further outbursts were reported on 8 July (in x-rays) and 9 July (in visible wavelengths).

This series of pre- and post-impact natural outbursts bears strong resemblance to the one induced by the impact itself. The projected expansion velocity of the dust cloud has been ~200 m/s for every outburst. The coma morphologies induced by both the natural outbursts and the impact-induced one have been very similar. Specifically, the shape of the ejecta cloud and the ejecta opening angles (~180°) behave similarly,

expanding until the radiation pressure starts to dominate the structure.

Summary. The ground-based observing campaign brought together a collaboration of unprecedented size and scope for support of a spacecraft mission. We had worldwide international cooperation, which was critical for addressing fundamental questions revealed by the Deep Impact experiment. Data analysis continues, but several conclusions can be made.

We now have adequate observations to understand the detailed composition of dust in a Jupiter-family comet. Furthermore, this dust comes from deeper subsurface layers than normal, so it is less processed than the cometary dust we normally see. The dust to gas ratio in the ejecta was larger than what was measured before impact, which suggests that the volatile content of the nucleus's material is depleted even several meters below the surface.

The consensus from the observing campaign was that the impact was an impulsive event. A large amount of material was ejected into the coma in a very short time and took no more than 5 days to dissipate, but the amount of material emitted from the impact site was relatively small. Although we cannot conclusively state that the impact did not create a new source, we can conclude that any new source must be small when compared to the sources that already existed on the nucleus.

Fig. 4. Synoptic presentation of photometrically calibrated mid-IR fluxes as measured with the European Southern Observatory's 3.6-m telescope. Aperture size was 2500 km at the comet. Data were obtained from 2 days before impact to 7 days after impact. The scatter in the data is due to the "noise" introduced by the normal comet activity. This is consistent with observations done in February and March 2005 (17). Blackbody curves are drawn for each epoch to give an indication of the amount of "nonthermal" flux in the filters sensitive to solid-state features (at 9, 10, and 11 μm).
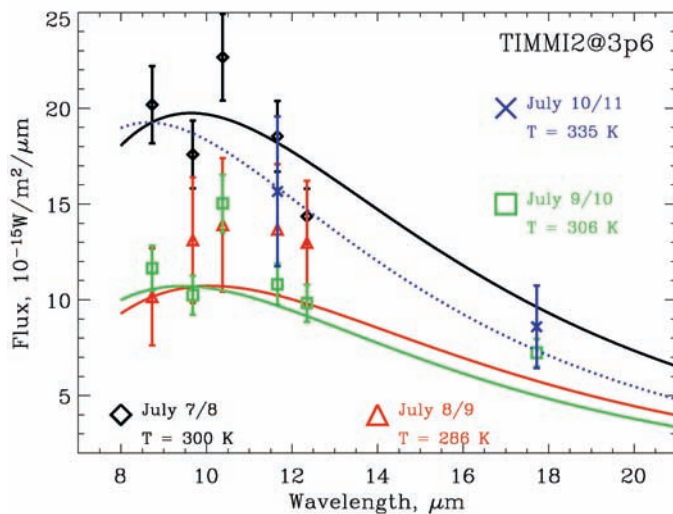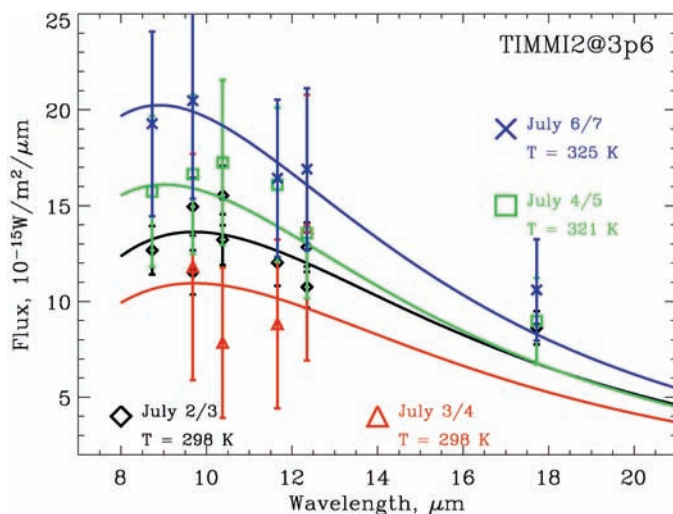
References and Notes

1. M. J. S. Belton et al., Space Sci. Rev. **117**, 137 (2005).
2. K. J. Meech et al., Space Sci. Rev. **117**, 297 (2005).
3. Note that for succinctness the term "Earth-based" is used to describe observations from ground-based telescopes, Earth-orbiting telescopes, and Sun-orbiting telescopes.
4. Z. Sekanina, H. Boehnhardt, Earth Moon Planets **78**, 313 (1999).
5. L. Lara et al., in preparation.
6. D. G. Schleicher et al., in preparation.
7. M. F. A'Hearn, R. L. Millis, D. G. Schleicher, D. J. Osip, P. V. Birch, Icarus **118**, 223 (1995).
8. M. J. Mumma et al., Science **310**, 270 (2005).
9. D. Hutsemekers et al., Astron. Astrophys., in press (available at http://arXiv.org/abs/astro-ph/0508033).
10. C. M. Lisse, T. E. Cravens, K. Dennerl, in Comets II, M. C. Festou et al., Eds. (Univ. of Arizona Press, Tucson, AZ, 2005), pp. 631–643.
11. C. M. Lisse et al., Space Sci. Rev. **117**, 161 (2005).
12. M. F. A'Hearn et al., Science **310**, 258 (2005); published online 8 September 2005 (10.1126/science.1118923).
13. S. Sugita et al., Science **310**, 274 (2005).
14. D. E. Harker, C. E. Woodward, D. H. Wooden, Science **310**, 278 (2005).
15. C. Lisse et al., Intl. Astron. Union Circ. 8571 (2005).
16. Amateur Monitoring by the Observadores_Cometas Group (http://astrosurf.com/somyce/c_cometas/9P/9P.htm).
17. H. U. Käufl et al., Intl. Astron. Union Circ. 8593 (2005).
18. Supported by the University of Maryland and by University of Hawaii subcontract Z667702, which was awarded under prime contract NASW-00004 from NASA. We thank telescope allocation committees everywhere, too numerous to list, for their generous support of time.

Fig. 5. Impact light curve taken from the charge-coupled device guide camera at United Kingdom Infrared Telescope, sampled at 20 Hz. The triple-slope phenomenon in the first few minutes after impact is clear. The data have been ratioed to the brightness at the time of impact.